UC Irvine
UC Irvine Previously Published Works

Title

Z -isomerization of retinoids through combination of monochromatic photoisomerization and metal catalysis

Permalink

Journal

ISSN

Authors

Kahremany, Shirin
Sander, Christopher Lane
Tochtrop, Gregory P
et al.

Publication Date

DOI

Peer reviewed

Z-isomerization of retinoids through combination of monochromatic photoisomerization and metal catalysis

Shirin Kahremany[*,1], **Christopher Lane Sander**[1,2], **Gregory P. Tochtrop**[3], **Adam Kubas**[*,4], **Krzysztof Palczewski**[*,1]

[1]Gavin Herbert Eye Institute and the Department of Ophthalmology, University of California, Irvine, California, USA 92697 [2]Department of Pharmacology, Case Western Reserve University, Cleveland, Ohio, USA 44106 [3]Department of Chemistry, Case Western Reserve University, Cleveland, Ohio, USA 44106 [4]Institute of Physical Chemistry, Polish Academy of Sciences, Kasprzaka 44/52, 01-224 Warsaw, Poland

Abstract

Catalytic *Z*-isomerization of retinoids to their thermodynamically less stable *Z*-isomer remains a challenge. In this report, we present a photochemical approach for the catalytic *Z*-isomerization of retinoids using monochromatic wavelength UV irradiation treatment. We have developed a straightforward approach for the synthesis of Z-retinoids in high yield, overcoming common obstacles normally associated with their synthesis. Calculations based on density functional theory (DFT) have allowed us to correlate the experimentally observed *Z*-isomer distribution of retinoids with the energies of chemically important intermediates, which include ground- and excited-state potential energy surfaces. We also demonstrate the application of the current method by synthesizing gram-scale quantities of 9-*cis*-retinyl acetate **9Z-a**. Operational simplicity and gram-scale ability make this chemistry a very practical solution to the problem of *Z*-isomer retinoid synthesis.

Graphical Abstract

Photoisomerization of therapeutic *cis*-retinoids using monochromatic UV light--tunable *via* photocatalysts and explained by DFT calculations.

Keywords

Photochemistry; retinoids; catalytic isomerization; UV irradiation; photocatalyst; rhodopsin

[*]To whom correspondence should be addressed: 1. Krzysztof Palczewski, Ph.D., Gavin Herbert Eye Institute, Department of Ophthalmology, University of California, Irvine, CA, USA 92657; kpalczew@uci.edu 2. Shirin Kahremany, Ph.D., Gavin Herbert Eye Institute, Department of Ophthalmology, University of California, Irvine, CA, USA 92697; skahrema@uci.edu 3. Adam Kubas, Ph.D., Institute of Physical Chemistry, Polish Academy of Sciences, Kasprzaka 44/52, 01-224 Warsaw, Poland; akubas@ichf.edu.pl.

Conflicts of interest

The authors declare no competing financial interests.

Introduction

Polyene retinoids are an important class of biologically active molecules involved in many facets of human physiology. Retinoids exist in the form of retinol, retinal, and retinoic acid and have functions in vertebrate growth and development, cell differentiation, [1] embryonic development, [2] vision, [3–5] the immune response, [6] and reproduction.[7] The geometric configurations of retinoids have enormous impact on their chemical and biological properties. For example, 13-*cis*-retinoic acid (isotretinoin) is used for the treatment of acne, and other retinoids are used to treat photo-damaged skin.[8] Isotretinoin also is currently used as a differentiating agent after chemotherapy and stem cell transplants in juvenile patients with neuroblastoma.[9] Retinoids have also been used as anti-cancer chemotherapeutic agents where they are thought to inhibit carcinogenesis at the initiation, promotion, and progression stages.[10–11] The anticancer activity of the retinoids is mainly due to their binding to nuclear receptors that act as hormone receptors activating target genes.[12]

The *Z*-isomeric form of retinal plays an important role in vision as a chromophore of rod and cone photoreceptor cells. The retinoid cycle consists of a series of biochemical reactions needed to regenerate the visual chromophore 11-*cis*-retinal to sustain vision. Genetic or environmental factors affecting chromophore production can lead to diseases of the retina and eventually blindness. Pharmacological interventions by means of *Z*-isomers of retinal and retinyl acetate are used to maintain vision in inherited retinal degenerative disease. [13–14] In light of these facts, synthetically tractable access to thermodynamically less stable *Z*-retinoids represents a critical need within the medical community.

We recently studied the *Z*-isomerization of all-*trans*-retinoids and developed a catalytic synthesis of 9-*cis* retinoids using transition metal-based reagents. We demonstrated that direct isomerization using readily available palladium-based catalysts in acetonitrile by conventionally-heated or microwave irradiation yields 30% 9-*cis*-retinoid in just one step.[15] In the course of subsequent studies of these reactions, with the intent of improving the yield, we have performed photochemical reactions to convert *E* retinoids to their corresponding *Z* isomers using single band wavelength irradiation (Scheme 1). The combination of photocatalyst compounds with ultraviolet (UV) irradiation in the *Z*-isomerization reaction has also been examined.

In general, photochemical reactions allow access to excited state potential energy surfaces. The initial fast, dipole-allowed photon absorption and electronic excitation create an excited state that has various decay channels including those leading to new chemical species provided the lifetime of the excited state is sufficient for the relaxation to occur. Such a reactive excited state path enables the thermodynamically unfavorable *E* to *Z* isomerization of olefins.[16–17] Photoisomerization of all-*trans*-retinal upon light excitation with different UV lamps has been studied previously[18], but these studies were only able to obtain the *Z*-isomer in modest yields. The key drawback of using UV lamps is their broad emission spectrum including emission in the infrared (IR) region, which significantly affects the final isomer distribution by uncontrolled high-energy vibrational state occupation. In comparison to UV lamps, light-emitting diodes (LEDs) have higher energy efficiency, more constant

light intensity, a longer lifetime, and are easier to control thermally.[19] The rationale for using single band wavelength LEDs was recently exemplified in a report wherein monochromatic wavelength LEDs showed higher efficacy for the production of vitamin D3 in the skin than broad-spectrum, natural sunlight.[20] Given their therapeutic relevance, it is necessary to develop more effective methods for the synthesis of Z-retinoids.[21]

Results and discussion

Optimization of Photoisomerization Conditions

In this study, we extend the substrate scope of the photochemical isomerization reaction to several retinoids. By using single band LEDs as our light source, we can now synthesize Z-retinoids in high yields. UV light irradiation of E-retinoids produces a diverse cis-retinoid composition with mono and di-cis products. In this report, we focus on Z-isomerization that leads to mono-cis products (**7Z, 9Z, 11Z and 13Z**) with mild steric hindrances. We also detail the synthesis of these compounds in large-scale. Importantly, the reaction conditions are mild, easily accessible, and operationally simple, such that use of the procedure detailed herein can be easily implemented by others.

A screen of monochromatic diodes with several wavelength bands (320, 385, 395, 405, 420, 505, 530, 625 nm) at room temperature over four hours was conducted to find the optimal wavelength for the production of Z-isomers using all-trans-retinyl acetate **E-a** as a test substrate. The optimal wavelength was 385 nm, and, after 4 h of reaction, the yield of 9-cis **9Z-a** reached 60% (Figure 1).

To further optimize the reaction conditions, we screened across common solvents for the Z-isomerization of all-trans-retinyl acetate **E-a**. As shown in Table 1, reactions in a nonpolar solvent (hexane), yielded low amounts of Z-isomers (entry 1). We then determined that in acetonitrile, **E-a** could be converted to the cis isomers **9Z-a** and **7Z-a** with a high conversion rate of 66% under irradiation at 385 nm (entry 2). The reaction also proceeded effectively in ethanol and ethyl acetate, and produced **9Z-a** in substantial yields (entries 3 and 4). Traces of water had negligible effect on the reaction, and cis isomers were obtained at a 64% conversion (entry 5). However, the conversion rate dropped to 27% if the water ratio increased (compare entries 5 and 6). The reaction performed in an air atmosphere showed the same yield as in a nitrogen atmosphere, apparently showing the absence of an oxygen effect (entries 2 and 7). A lower yield of **9Z-a** was also observed when shorter or higher wavelengths of light were used (entries 8–10). In addition, DMSO acting as a free radical scavenger did not inhibit the Z-isomerization and yielded 51% **9Z-a** after a 1 h reaction (entry 11). Notably, no **9Z-a** was observed in the absence of UV exposure, verifying that UV light was essential for the productive chemistry (entry 12).

Reaction progress was followed via HPLC, and provided additional, independent verification of the efficacy of the isomerization triggered by the UV irradiation at 385 nm. HPLC analysis indicated that **E-a** was effectively isomerized to the major isomer **9Z-a** with no photodegradation products (Figure 2A). Hence, acetonitrile was used as the solvent in order to promote the creation of the **9Z-a** isomer at 385 nm, the optimal wavelength.

Characterization and Modulation of the Photoisomerization Reaction

In these optimal conditions (acetonitrile as a solvent and UV irradiation at 385 nm), we also studied the concentration and energy dependence of the reaction. The yield of 9-*cis* is stable through an increasing amount of substrate, up to 1 mM, but dramatically decreases above this concentration, most probably due to the inner filter effect, in which the excitation beam is attenuated by highly concentrated solution (Figure 2B).[22] The amount of 9-*cis* obtained also increases with the increasing energy of incoming light, and reaches the highest yield of **9Z-a** at 1.5×10^5 mW/h (Figure 2C).

To evaluate the equilibrium rate, the reactions of isolated all-*trans* (**E-a**), 9-*cis* (**9Z-a**) and 13-*cis* (**13Z-a**) isomers were monitored over time (Figure 3). We found that the equilibrium is shifted towards the *cis* isomer, and the rate of isomerization to **9Z-a** is greater than the isomerization to the *trans* isomer (Figure 3). This shift in the equilibrium causes the buildup of 9-*cis* to reach 60% after 4 h, with all-*trans* formation stably kept around 20%. The isomerization of the minor isomer 13-*cis* shows that the reaction is in equilibrium with the 9, 13-*dicis* isomer, with no conversion to **E-a** (Supporting Information, SI Figure S3).

In addition, to elucidate the nature of the observed *Z*-isomerization, quenching experiments were performed using **E-a** in acetonitrile. The addition of TEMPO, a radical quencher, had no inhibitory effect on the *Z*-isomerization reaction (Figure 3). Moreover, the formation of the *cis* isomers appears to be favored in solvents with high dielectric constants like acetonitrile and ethyl acetate, as shown in Table 1. Based on these results and previous studies, it is likely that the excited state proceeds through a singlet pathway with zwitterionic characteristics.[23–24]

We next investigated the scope and limitations of the *Z*-isomerization reaction under the optimized conditions at several wavelengths (320, 385, 395, 405, 420, 505, 530, 625 nm). Our investigation was conducted using three representative retinoid molecules (all-*trans*-retinoic acid **E-b,** all-*trans*-retinol **E-c**, and all-*trans*-retinal **E-d**) as a substrate. An excellent *E*/*Z* ratio was achieved after just 1 h of reaction, and each retinoid showed a unique wavelength at which its conversion was the highest. The results summarized in Table 2 show the most effective UV wavelength for each retinoid and the difference in distribution of the *Z*-isomers. All-*trans*-retinoic acid **E-b** was converted to the corresponding *cis*-isomers in a good yield with a ratio of 1:0.6:1.2 for 9-*cis*:13-*cis*:11-*cis*-retinoic acid (entry 1). The all-*trans*-retinol **E-c** reaction afforded the corresponding 9-*cis* isomer **9Z-c** with an excellent *E*/*Z* ratio (entry 2). All-*trans*-retinal **E-d** was converted to *cis* isomers in a ratio of 1:0.1:1.3:1.7 for 9-*cis*:7-*cis*:13-*cis*:11-*cis* (**9Z-d**: **7Z-d**: **13Z-d**: **11Z-d**).

Isomer Selection via Addition of Metal Catalyst

While these data demonstrate that direct excitation of retinoids is possible, photoisomerization using a small-molecule catalyst is considered efficient and allows for selective activation of specific functional groups. This strategy has been demonstrated using an Ir(III) complex to expedite the *E* to *Z* isomerization of activated olefins *via* an energy transfer mechanism.[25–26] To improve the *cis* isomer yields and clarify the reaction mechanism, we used several catalysts (**I-IV**, see reaction scheme associated with Table 3) to

explore their effect under irradiation by a monochromatic wavelength LED and quantified the yield of *cis* isomers. Catalysts **I**- **II** were used due to their effectiveness in producing the *cis*-retinoid using conventional heating or microwave irradiation based on our previous report.[15] In addition, riboflavin (catalyst **IV)** was reported to catalyze the *E→Z* photoisomerization of retinal.[27] However, these compounds did not increase the yield of *Z*-isomers in our current system. Only Ir-based catalyst **III** affected the *Z*-isomerization reaction, and the distribution of *cis* isomers was driven toward the formation of the 13-*cis* isomer at the expense of 9-*cis* formation (Table 3). The reaction of **E-a** with catalyst **III** (5 mol %) in CH$_3$CN for 1 h in 385 nm light yielded a 13-*cis*:9-*cis* ratio of 3:1 vs 0.1:1 in the absence of catalyst. (Table 3, entry 1). Retinoids **E-b** and **E-d** isomerization yielded moderate changes in the distribution of 13-*cis* and 9-*cis* compared to the catalyst-free reaction with a ratio of 1.1:1 and 1.6:1, respectively (entries 2, 4). Isomerization of retinoid **E-c** with catalyst **III** also showed inhibition of the 9-*cis* isomer (entry 3).

Analysis of the Light/Catalyst-driven Reaction

We subsequently performed kinetic studies for both *E* and *Z* (9- and 13-*cis*) isolated isomers of retinyl acetate in the presence of catalyst **III**. Isomerization of *E* to *Z* showed that the concentration of 9-*cis* isomer **9Z-a** decreases as the concentration of catalyst increases. Conversely, the yield of 13-*cis* increased with an increase of the catalyst (Figure 4A). When the isomerization of 9-*cis* to *E* was performed, both products, all-*trans* and 13-*cis*, showed an increase as the concentration of catalyst was increased (Figure 4B). Additionally, isomerization of 13-cis to *E* showed an increase in the amount of all-*trans* and a decrease in 9-*cis* as the concentration of the catalyst increased (Figure 4C). These results show that the distribution of the *cis* isomers changes with the addition of the catalyst to produce the 13-*cis* isomer along with the thermodynamically stable *E* isomer, which could indicate a different mechanism of reaction when the catalyst is present.

We also tried to clarify whether the isomerization in the presence of catalyst **III** involves a radical-based mechanism. Addition of TEMPO led to suppression of 13-*cis* isomer formation, shifting the largest portion of product to the 9-*cis* isomer, as is the case of the standard reaction condition in the absence of catalyst, suggesting that a triplet state of catalyst **III** (delocalized biradical intermediate) might be involved in this reaction.

Quantum Chemical Analysis of Reaction Mechanism

To understand the distribution of the products, we first considered the structure of the tested molecules. Retinal and retinoic acid have a scaffold of push-pull olefin, with marginally longer double C=C and shorter single C-C bonds as compared to retinol and retinyl esters, which have donating groups at the end of the polyene chain (see Table 4). Although bond lengths generally correlate with bond strengths, small differences observed between the two groups of molecules cannot by itself explain the distribution of major products in a photochemical reaction that is governed by steric and electronic effects of the entire molecule. We note, however, that according to our calculations the vertical excitation involves mainly highest occupied molecular orbitals (HOMO) and lowest unoccupied molecular orbitals (LUMO) of the respective molecules. These are delocalized over the entire π-bond system. In order to understand the product distribution, one needs a way to

predict how much energy will be "stored locally" in each double bond upon excitation. Recall that strong absorption is a result of a dipole-allowed electronic transition. Carbon-carbon double bonds can be viewed as isolated dipoles as the charge distribution at two carbon atoms is unequal. We now consider only HOMO orbitals (essentially a linear combination of *2p* orbitals) and partition them into percentage contributions that come from each carbon atom of the conjugated chain using a Löwdin population scheme.[28] The absolute difference between the contributions of carbon atoms that form a bond is a "local polarization of the bond" (LPB) that should be proportional to a "local dipole moment". The same decomposition can be carried out for LUMO orbitals. We now consider the relative local polarization change upon HOMO → LUMO excitation ($LPC_{HOMO \rightarrow LUMO}$):

$$LPC_{HOMO \rightarrow LUMO} = \left(\left| \left(LPB_{HOMO} - LPB_{LUMO} \right) \right| / \left| LPB_{HOMO} \right| \right) * 100 \ \%$$

for each carbon-carbon double bond (Table 4). Large $LPC_{HOMO \rightarrow LUMO}$ values mean that a large portion of the energy will be stored in a given bond. The $LPC_{HOMO \rightarrow LUMO}$ value for 9-*cis*-retinyl acetate is 187.5 % and at least three times larger than $LPC_{HOMO \rightarrow LUMO}$ for other isomers of retinyl acetate. This determines the major product of the photoisomerization reaction. On the other hand, for retinal the $LPC_{HOMO \rightarrow LUMO}$ values are comparable for 11-*cis* and 13-*cis* isomers (57.9 and 94.4 %, respectively) with the other two isomers also exhibiting a significant value of $LPC_{HOMO \rightarrow LUMO}$ of about 22%. Thus, our simple model predicts correctly a mixture of isomers as an outcome of the reaction.

The LPC method can be viewed as a one electron/two orbital model that accounts only for the initial and final states and is thus related to the thermodynamics of the examined reactions. It lacks any wavelength dependency and cannot be used to track the potential role of the triplet states. Thus, in order to gain further insight into the processes that govern the product distribution of the photochemical reactions we carried out extensive quantum chemical calculations at the density functional theory (DFT) level to explore the potential energy surfaces of the examined molecules. Most of the previous theoretical studies focused on the biologically relevant isomerization of all-*trans* to 11-*cis* retinoid derivatives. There is strong evidence that such a process in the opsin-embedded chromophore proceeds *via* the conical intersection between the excited singlet state (S_1) and ground state singlet (S_0).[29] Johnson et al. showed both experimentally and theoretically that the key molecular modes responsible for the *E/Z* isomerization reaction involve C=C stretching and twisting around carbon-carbon double bonds.[30–31] Earlier, Frutos et al. arrived at the same conclusion. However, the theoretical model did not include any explicit nonadiabatic couplings and the $S_1 \rightarrow S_0$ decay probability was estimated with a simple Landau-Zener model.[32] The studies emphasize that the biological *E/Z* isomerization occurs very fast (~100 fs), but this is a consequence of chromophore binding pocket geometry and protein dynamics that increase the energy of the ground state and at the same time force selected bond twists.

According to Figure 3, the equilibration in our current case occurs on the hour time scale, thus predicting the final composition based on pure non-adiabatic molecular dynamics seems to be almost impossible. Instead, we decided to develop a model that captures all chemically important intermediates at the three potential energy surfaces: ground state

singlet (S_0), excited state singlet (S_1), and triplet (T_1) and present the results in the form of Jablonski diagrams in Figure 5. Our calculations focused on two substrates with a different number of conjugated bonds: retinyl acetate (**E-a**, Figure 5A) and retinal (**1d**, Figure 5B). The primary product of the *E*/*Z* isomerization of the former is the 9-*cis* isomer (with some traces of 7- and 13-*cis*), while the latter yields a mixture of 9-, 11- and 13-*cis* isomers.

We assumed that the reaction proceeds *via* multiple intermediates in an overall reversible way, thus in the course of the reaction both *trans* and *cis* ground state isomers undergo photochemical transformations. After electronic excitation, the system either decays *via* a fluorescence channel or the molecular framework could evolve to yield a conical intersection and then switch to a ground state potential energy surface. Location of conical intersections requires a general knowledge of non-adiabatic couplings and requires multireference treatment of the underlying electronic structure. According to the recent work of Gozem et al., dynamic electron correlation effects play a major role in proper treatment of both but are extremely intensive to compute, especially if molecular dynamics is to be considered.[33] To avoid such complications and stay at the DFT level, we note that the true conical intersection between the S_1^{trans} state and any of the S_0^{cis} states involves closed shell singlet (S_0) and open-shell singlet (S_1) wave functions. The latter can be described at the DFT level approximately with the broken symmetry (BS) approach.[34–35] Geometry relaxation of the BS state leads unavoidably to a ground state structure as the Cartesian energy gradients are those of the ground state. In contrast, we expect gradients of the T_1 state to be a good approximation of the true S_1 Cartesian energy derivatives. In addition, energies of T_1 and S_1 should be very close as they only differ by the exchange interactions. Thus, we approximate conical intersection geometry with the so-called minimum energy crossing point (MECP) approach between the broken-symmetry S_1 and triplet T_1 states. In this way we allow for full system relaxation in the direction of crossing but bias the gradients so that the structure does not collapses to the S_0 state. An additional advantage of using such defined MECP geometries is that they naturally correspond to intermediate states in the intersystem crossing (ISC) between triplet and singlet states of interest. The full protocol for obtaining these intermediate states (MECP and triplet transition states for rotation, T^{TS}) is provided in the Experimental section.

As shown in Figure 5A, retinyl acetate has a computed vertical λ_{max} at 327 nm (S_1 energy of 80.2 kcal/mol), while retinal **E-d** has an overall, lower-lying excited state manifold with λ_{max} at 380 nm (S_1 energy of 69.8 kcal/mol). The corresponding T_1 adiabatic states are 34.1 kcal/mol and 29.0 kcal/mol, respectively. The fluorescence rate of S_1^{trans} of the retinal is slightly lower (k_{fluor} =6.0 × 10^8 s^{-1}) than the k_{fluor} of retinyl acetate (9.6 × 10^8 s^{-1}). This observation along with the lower energy of the triplet state makes the T_1 state of the retinal **E-d** population more probable than retinyl acetate **E-a**. The latter is expected to proceed on the S_1 potential energy surface (PES) and relax to one of the MECP geometries from which the S_0 surfaces of four of the *cis* isomers are accessible. As shown in Figure 5 and Table S1, MECP-9-*cis* that connects S_1^{trans} and S_0^{cis-7} has the lowest energy, MECP-7-*cis* and MECP-13-*cis* are lower by 2 kcal/mol, and MECP-11-*cis* is 2.5 kcal/mol higher in energy. It should be noted that the order of the MECP geometries coincides with the distribution obtained experimentally.

In the case of retinal the density of low-lying MECP structures is high. MECP values for 7-*cis*, 9-*cis* and 11-*cis* lie essentially in a 1 kcal/mol energy window, while 13-*cis* is slightly greater. Interestingly, the density of the transition states that correspond to the rotation around the C=C bonds in the triplet state (T^{TS}) is also very high, higher than those of retinyl acetate. Most of these T^{TS} states are in resonance with MECP states. These findings point to the possibility that a triplet path is operative. Figure 5 provides a clear indication that 7-*cis*, 9-*cis* and 11-*cis* should be the major products of the reaction. However, 13-*cis* is a thermodynamic product of the reaction, as $T_1^{13\text{-}cis}$ is only 2.4 kcal/mol greater than the most stable $T_1^{11\text{-}cis}$ isomer. Experimentally, 9-*cis*, 11-*cis* and 13-*cis* are major products in the case of retinal with 7-*cis* being a minor product. One possible phenomenon which is missing in our calculations is the dynamic interactions of the carbonyl group with the solvent molecules that could further stabilize the 13-*cis* isomer.[36] On the other hand, such interactions could hinder β-ionone moiety rotations necessary to accommodate 7-*cis* geometry.

In addition, our experimental results suggest a wavelength dependency of 9-*cis*-retinyl acetate **9Z-a** yield, which requires further clarification (Figure 1A). Remarkably, the most optimal wavelength is 385 nm, 60 nm longer than λ_{max} for all-*trans* isomer. The key effect that generates the S_1^{trans} population at lower excitation energies is the population of higher vibrational states of the ground state as well as the dynamic motion of the molecule. Among the *cis* isomers, 9-*cis* **9Z-a** has a 12 nm lower first excitation energy (315 nm). Thus, the use of high-energy UV LED ca. 320 nm would very efficiently depopulate the desired product **9Z-a**. According to our Jablonski diagram, the decay of $S_1^{9\text{-}cis}$ leads to MECP and then either to the all-*trans* substrate or back to 9-*cis* product. With well-tuned excitation energy (327 nm) the excitation of all-*trans* species populates the S_1^{trans} very efficiently. High concentration of the S_1^{trans} allows for the triplet path to be operative. Here, the path that leads to 9-*cis* product is no longer lowest in energy so that other isomers will be produced in higher rates. The argument of triplet path opening upon use of tuned excitation energy can be also used in the case of all-*trans*-retinal **E-d**. In this case, the best wavelength was found to be 395 nm, very close to the optimal 380 nm, and the variation of product distribution with various wavelengths was not significant. In contrast to retinyl acetate, the manifold of the triplet transition states T^{TS} is almost the same as the MECP states. Thus, both paths will provide similar product distribution and provide low sensitivity to wavelength choice.

Next, we performed the calculations with retinyl acetate **E-a** and catalyst **III** as a representative system for photocatalytic activity (see Table 3). The iridium catalyst **III** constitutes a challenge for computational chemistry, due to the number of atoms and the dense manifold of the excited states. We optimized the structures of the catalyst in a cationic isolated form as well in the complex with the retinyl acetate. We found that retinyl acetate interacts with the catalyst favorably *via* π-π and dispersion forces (B3LYP+D3BJ/def2-TZVP interaction energy of −18.4 kcal/mol) that bring the carbonyl oxygen atom in close contact with the ligand (shortest O…C distance of 3.1 Å, O…Ir distance is 4.5 Å). The true interaction energy is probably less negative, due to omitted solvent effects, and the reported value should be considered as an upper limit. The calculated UV-VIS spectra for the separate substrates and the complex match well with the experimental spectra (Figure 6). In line with experimental observations, the most intense band, corresponding to π- π* excitation of the

retinyl acetate, is shifted to higher energies by about 8 nm upon complexation. This is primarily due to polyene chain deformation and coulombic interactions with the positively charged iridium center. Interestingly, the calculated spectrum of the complex features a low-lying (~430 nm) excited state of low intensity. We identified it as a charge-transfer (CT) state from the retinyl moiety into the catalyst orbital system. This is further confirmed experimentally by the fact that the band between 400 and 500 nm gains significant intensity and becomes broader as compared to the parent catalyst spectrum. This suggests that upon irradiation an electron transfer could occur from the retinyl acetate to catalyst **III** so that the *E*/*Z* isomerization would in fact proceed in a cationic state of the chromophore. However, this does not exclude an energy transfer mechanism in parallel as the electron transfer reactions heavily depend on the solvent and dynamic distance between donor and acceptor molecules.

Irrespective of changes in the UV-Vis spectrum upon complexation, we predict that complexation alters the dynamics of the retinyl acetate as compared to the free molecule. We speculate that the closest $C^{13}=C^{14}$ bond will be most influenced due to direct interaction with oxygen from the ester moiety that directly interacts with the positively charged catalyst. This could result in increased 13-*cis* product formation as observed experimentally.

Although the exact reaction mechanism is still unknown, based on the experimental and theoretical results described above and reports in the literature[1], we propose a mechanism for the *Z*-isomerization of all-*trans*-retinyl acetate *E*-**a** (Scheme 2). Photoisomerization of *E*-**a** with a monochromatic wavelength LED produces higher yields of 9-*cis* isomer. It could be explained by the zwitterionic characteristic of the S_1 excited state and a uniform distribution of the partial charge on both sides of the C^9-C^{10} bond of the excited polyene, leading to the more stable 9-*cis* conical intersection intermediate (MECP). In the presence of catalyst **III**, a unique interaction with the retinyl acetate produces a complex in which the electron rich moiety of the substrate is in proximity to the Ir metal of the catalyst. In this way, the triplet state of the (Ir(III)*) transfers the energy to the closest $C^{13}=C^{14}$ bond of the substrate leading primarily to the 13-*cis* isomer.

Biochemical Study of Product Uptake by a Physiological Receptor

To further demonstrate the practicality of this one-pot protocol, we performed a regeneration assay with opsin protein (OPS) in rod outer segment (ROS) membranes with all-*trans*-retinal *E*-**d** using time-dependent UV-Vis spectroscopy. Addition of *E*-**d** (4.7 nM) to OPS and irradiation at 395 nm at several time points (5–15 min) resulted in the Schiff base formation at 489 nm between OPS and *cis* isomers of *E*-**d**. (Figure 7). Thus, this method could be used for *in vitro* studies of opsin proteins binding different analogues of retinoids.

Gram-scale Synthesis

To further explore the practicality of our methods, a gram-scale reaction of all-*trans*-retinyl acetate *E*-**a** was performed in a quartz round bottom flask using a 30 W, 385 nm UV LED, and monitored over 24 h. Using this preparative photochemistry set up, [37–38] the transformation produced the 9-*cis*-isomer **9Z-a** in 80% yield (Scheme 3). This finding demonstrates that our protocol is scalable and thereby permits more comprehensive

therapeutic testing in various disease models, including retinal degenerative diseases in murine and canine models, [39–42] as a prelude to human investigations.

Conclusions

Until recently, the direct *Z*-isomerization of retinoids was limited by low yields. Here, we report the first direct *Z*-isomerization using a monochromatic irradiation system. We have developed a straightforward approach for the synthesis of *Z*-retinoids in high yield, overcoming common obstacles normally associated with their synthesis. We also presented DFT computations for retinyl acetate *E*-**a** and retinal *E*-**d** isomerization by monochromatic UV light. Two independent approaches were then applied to explain the distribution of isomers: a simple orbital-based relative local polarization change model and a model that focuses on the energy of the excited state intermediates. The outcomes of these two approaches were complementary and explain the observed product distributions. Moreover, we demonstrated that retinyl acetate interacts strongly with the iridium-based catalyst, and this interaction accounts for the major product switch. Additionally, we presented findings further validating the current method by synthesizing gram-scale quantities of 9-*cis*-retinyl acetate **9Z-a**. This method is of interest from the perspective of green chemistry and ease of gram-scale synthesis for large-scale tests of therapeutic capabilities in retinal degenerative models, among other therapeutic uses.[39–42] Further optimization of the methodology, as well as investigations into the scope and mechanism of the transformation, should be pursued. Particular focus should be aimed at modifying the catalyst to produce the 11Z isomer. Such a catalyst might recreate the microenvironment of the native binding pocket of receptors able to regenerate the visual chromophore.[43] Future study on this topic could uncover insights in both chemistry and biology.

Experimental

All reagents, catalysts, and standard retinoids were obtained from commercial suppliers (Sigma Aldrich, St. Louis, MO and Toronto Research Chemical, Toronto, Canada) and used without any further purification, unless otherwise noted.

Nuclear Magnetic Resonance (NMR) Spectroscopy

The NMR spectra were recorded on a Bruker 500 MHz and 800 MHz apparatus at 25 °C and referenced relative to the residual proton resonances of C_6D_6 (δ = 7.16 ppm). ^1H NMR spectra of the compounds were collected with their corresponding 2D nuclear Overhauser effect spectroscopy, and heteronuclear single quantum coherence (HSQC) spectroscopy. Spectra were processed using the MestReNova package.[44] The coupling constants (J) are reported in Hertz (Hz).

High Performance Liquid Chromatography (HPLC) Analysis

Procedures were performed under dim red light. Retinoids were stored in *N,N*-dimethylformamide under argon at −80 °C. Retinoid analysis was performed on an Agilent 1200 series HPLC equipped with a diode array detector and Agilent Chemstation A.10.01 software (Agilent, Palo Alto, CA). A normal phase column (Beckman Ultrasphere Si 5μ, 4.6

× 250 mm [Beckman Instruments, Fullerton, CA]) and an isocratic solvent system of 2–10% ethyl acetate in hexane (v/v) were used at 20 °C and a flow rate of 1.4 ml/min. In addition, a reverse phase column (C18, 4.6 × 250 mm, 5 μm, Phenomenex, Torrance, CA) and an isocratic solvent system of 40% (v/v) CH_3CN in aqueous 0.1% trifluoroacetic acid (TFA) was used at a flow rate of 1 ml/min at 20 °C. For retinal, retinal derivatives, retinol and retinyl acetate, the analyses were performed at 325 nm. Retinoic acid analysis was performed with detection at 355 nm.

All HPLC measurements were calibrated using standards of all-*trans*-retinoids, 9-*cis*-retinoids, 13-*cis*-retinods and 11-*cis*-retinoids.

Photochemical reactions

Photochemical reactions were carried out by dissolving 0.1 mmol of the retinoids in 2 mL acetonitrile. Reactions in the presence of catalysts were performed by dissolving 0.1 mmol of the retinoids and 1.4 μmol of the catalysts in 2 mL acetonitrile. The resulting mixtures were transferred to cuvettes (Starna Cells, Atascadero, CA, path length 1 mm) and illuminated using two different light sources. The samples were initially irradiated using a 300 W Xe arc lamp adapted with a wide band-pass filter (MAX-350, Asahi Spectra, Co., Ltd, CA, USA) or narrow band-pass filters for use at 320 nm. A second, LED light source (Thor Labs, Newton, NJ) was used over a wavelength range of 385 nm to 625 nm. After the treatment, the sample was dissolved in hexane and analyzed by HPLC.

For mechanistic studies, the reactions of all-*trans*-retinyl acetate **E-a** (0.1 mmol) in the presence and absence of 5 mol % catalyst **III**, in CH_3CN at 385 nm were performed in the presence of TEMPO (2,2,6,6-tetramethyl-1-piperidinyloxy), 1, 5 and 10 mol %, and monitored by HPLC for 1 h.

Kinetic studies

A stock solution of all-*trans*-retinyl acetate **E-a**, 9-*cis*-retinyl acetate **9Z-a** and 13-*cis*-retinyl acetate **13Z-a**, 0.1 mmol, and catalyst **III**, 0.1–1.5 μmol, were prepared. All manipulations were done under dim light, and the reactions were performed in a quartz cuvette. The reactions were performed in the presence and absence of catalyst **III.** Reactions in the presence of catalyst were performed in five conditions with **E-a**, **9Z-a** and **13Z-a** and dilutions of catalyst **III** in CH_3CN at 385 nm for 1h. After the reaction, a small aliquot of 10 μL was removed and added to a mixture of 100 μL H_2O and 50 μL of hexane. After extraction, 10 μL of the hexane layer were injected into the HPLC to monitor the change in products absorbance at λ=360 nm.

Large-scale synthesis of 9-cis-retinyl acetate (9Z-a)

A solution of all-trans-retinyl acetate **E-a** (2.1 gr, 7.3 mmol) in acetonitrile (400 mL) in a quartz round bottom flask was irradiated with 6 units of a 30 W, 385 nm UV LED. The reaction was performed in a darkroom for 24 h at room temperature. The resulting solution was dissolved in water (600 mL) and extracted with hexane (3 × 80 mL). The combined hexane layer was dried over $MgSO_4$ and evaporated under reduced pressure. Purification by

silica gel column chromatography (ethyl acetate/hexane 3:97) afforded 1.5 g (80%) of compound **9Z-a** as a yellow powder.

Preparation of opsin membranes

All experimental procedures were carried out in a darkroom under dim red light (>670 nm). Bovine rod outer segments (ROS) were prepared as described elsewhere.[45–47] ROS were washed with isotonic and hypotonic buffer to remove both soluble and membrane associated ROS proteins.[45] Purified ROS membranes (19.3 mg ml^{-1} Rhodopsin) were bleached with a 100 W white light for 30 min in the presence of 20 mM hydroxylamine. Bleached ROS/opsin membranes then were washed six times each with 35 ml of buffer containing 67 mM potassium phosphate, pH 7.0, 1 mM magnesium acetate, 0.1 mM EDTA and 1 mM dithiothreitol to dispose of excess hydroxylamine.

Binding assays with opsin

Opsin membranes at the final concentration of 3.4 μM were solubilized in buffer containing 20 mM Bis-Tris-Propane, pH 6.9, 100 mM NaCl and 0.1% n-dodecyl β-D-maltoside (DDM). Absorption spectra of solubilized opsin membranes were measured with a Cary 50 UV-Vis spectrophotometer maintained at 20 °C (TC 125 temperature controller, Quantum Northwest Inc., WA, USA). All-*trans*-retinal was added to the preparation of opsin membranes to achieve a final concentration of 37.5 μM and then illuminated with a single UV band at 385 nm at 20 °C for 15 min. Absorption spectra were measured every 5 min.

Quantum chemical calculations

All calculations were performed using the ORCA 4.1.2 program within the unrestricted density functional theory (DFT) formulation using a B3LYP exchange-correlation function that was corrected for dispersion interactions with a D3BJ pair-wise potential.[48–53] A triple-ζ quality def2-TZVP basis set was consistently employed throughout the study including a corresponding effective-core potential for the Ir atom.[54] Coulomb integrals were efficiently evaluated with the resolution of identity (RI) approximation using a def2/J auxiliary basis set.[55–56] Calculations of exchange integrals were sped-up by the chain-of-spheres semi-numerical integration techniques (COSX approximation).[57] The DFT integration grid was set to grid4 while COSX integration was gridx5 in the ORCA nomenclature. All ground-state geometries were subject to analytical second derivative calculations and were verified to possess only positive normal modes. Cartesian coordinates of all key intermediates can be found in the **SI**.

Computations of vertical excitation energies as well excited state geometry optimizations were carried out with the time-dependent density functional theory (TD-DFT).[58–59] To obtain UV-Vis spectra of the isolated iridium complex **III** and its adduct with the retinyl acetate we employed the recently developed simplified TD-DFT (sTD-DFT) approach of Bannwarth and Grimme.[60] We note that the method provides virtually identical spectra for the retinyl acetate as compared to the canonical implementation (see SI Figure S6). Absorption wavelengths in Figure 6 were uniformly shifted by −30 nm in order to match the experimental λ$_{max}$ of the retinyl acetate. Such a shift accounts only for systematic overstabilization of excited states in the TD-DFT method and does not influence properties

of the computed states. Fluorescence rates were computed with the path integral approach as implemented in the orca_esd module of ORCA.[61] In this theory, one has to make a choice regarding the approximation for the excited state potential energy surface. We decided to use the simplest approach, i.e. vertical gradient (VG). Here, the excited state geometry is approximated with one Quasi-Newton step that employs an exited state gradient and ground-state Hessian (GSH) at the ground-state geometry. Then, the Hessian of the excited state is made equal to the GSH.

MECP and T^{TS} structures were obtained in a multi-step procedure:

1. Constrained ground-state singlet geometry optimizations (relaxed scans) were carried out on structures where one selected dihedral angle (transition mode, Θ) was changed from 0° to 180° with 10° steps in a similar way as in our previous work.[15] This generated potential energy surface (PES) cuts along C^7-C^8, C^9-C^{10}, C^{11}-C^{12}, C^{13}-C^{14} double bond rotations. In all cases the maximum energy corresponded to Θ=90°.

2. At the maximum energy structures (Θ=90°) we performed excited state geometry optimizations keeping Θ=90° constant. These calculations typically exit with an error after about 20 iterations due to issues of the TD-DFT approach with the conical intersection points at the PES.

3. Each partially relaxed structure from point (2) was subject to two single-point calculations: at the high-spin (HS) triplet PES and at the broken-symmetry (BS) singlet PES. The latter reflects the electronic structure of the S_1 state but computed with a ground-state method. We note that at this point the relaxation of the BS state leads to ground-state structure with the unpaired density of essentially zero everywhere in space (closed-shell singlet geometry). Constrained relaxation of the HS state leads to transition states reported as T^{TS} in Figure 6.

4. The two states (HS and BS) are employed in the **MECP** geometry optimization with the method of Harvey et al.[62] Note that at this stage no geometry constraints are employed.

Characterization of the products

9-*cis*-retinyl acetate *E*-a ^{1}H NMR (500 MHz, C_6D_6) δ (ppm) 7.02–6.84 (m, 2H), 6.31(d, J= 15.9 Hz, 1H), 6.20 (d, J= 15.1 Hz, 1H), 6.03 (d, J= 11.4 Hz, 1H), 5.61 (t, J= 7.3 Hz, 1H), 4.61(d, J= 7.3 Hz, 2H), 1.96–1.91 (m, 5H), 1.79 (s, 3H), 1.66 (s, 3H), 1.57–1.53 (m, 5H), 1.46– 1.43 (m, 2H), 1.10 (s, 6H). ^{13}C NMR (126 MHz, C_6D_6) δ 170.08, 138.94, 138.54, 136.10, 134.97, 130.71, 129.64, 129.61, 128.90, 125.67, 124.75, 61.14, 39.81, 34.53, 33.26, 29.19, 22.07, 20.53, 19.67, 12.53.

NMR assignment was previously reported.[63]—7-*cis*-retinyl acetate **7Z-a** ^{1}H NMR (500 MHz, C_6D_6) δ (ppm) 7.01–6.89 (m, 2H), 6.28(d, J= 15.8 Hz, 1H), 6.26 (d, J= 15.0 Hz, 1H), 6.00 (d, J= 12.3 Hz, 1H), 5.72 (t, J= 7.3 Hz, 1H), 4.61(d, J= 7.3 Hz, 2H), 1.94–1.90 (m, 5H), 1.83 (s, 3H), 1.62 (s, 3H), 1.57–1.53 (m, 5H), 1.46– 1.43 (m, 2H), 1.10 (s, 6H).

13-*cis*-retinyl acetate **13Z-a** ¹H NMR (500 MHz, C₆D₆) δ (ppm) 6.72–6.63 (m, 2H), 6.30(s, 2H), 6.16 (d, *J*= 9.3 Hz, 1H), 5.48 (t, *J*= 7.4 Hz, 1H), 4.75(d, *J*= 7.3 Hz, 2H), 1.97 (t, *J*= 6.4 Hz, 2H), 1.84 (s, 3H), 1.79 (s, 3H), 1.76 (s, 3H), 1.67 (s, 3H), 1.61–1.56 (m, 2H), 1.51– 1.42 (m, 2H), 1.13 (s, 6H). ¹³C NMR (126 MHz, C₆D₆) δ 169.71, 138.00, 137.88, 137.45, 136.74, 130.84, 129.18, 128.52, 127.07, 123.61, 59.85, 39.62, 34.22, 32.99, 28.84, 21.61, 20.53, 20.05, 19.37, 12.39.

NMR assignment was previously reported.[63]—*9-cis-retinol* **9Z-c** ¹H NMR (500 MHz, C₆D₆) δ 7.01 (d, J = 16.1 Hz, 1H), 6.91 (dd, J = 15.1, 11.4 Hz, 1H), 6.33 (d, J = 16.0 Hz, 1H), 6.25 (d, J = 15.1 Hz, 1H), 6.09 (d, J = 11.3 Hz, 1H), 5.58 (t, J = 6.8 Hz, 1H), 3.96 (d, J = 6.7 Hz, 2H), 1.94 (s, 5H), 1.87 (d, J = 15.5 Hz, 1H), 1.81 (s, 3H), 1.57 (dd, J = 7.6, 4.3 Hz, 2H), 1.54 (s, 4H), 1.49 – 1.42 (m, 2H), 1.11 (s, 6H).

Complete NMR assignment was previously reported.[64]—*of 9-cis-retinal* **9Z-d** ¹H NMR (400 MHz, CDCl₃) δ 10.09 (d, *J* = 8.2 Hz, 1H), 7.22 (dd, *J* = 15, 11.6 Hz, 1H), 6.66 (d, *J* = 15.8 Hz, 1H), 6.33 (d, *J* = 15.8 Hz, 1H), 6.30 (d, *J* = 15 Hz, 1H), 6.09 (d, *J* = 11.6 Hz, 1H), 5.97 (d, *J* = 8.2 Hz, 1H), 2.31 (s, 3H), 2.05 (m, 2H), 2.02 (s, 3H), 1.75 (s, 3H), 1.64 (m, 2H), 1.48 (m, 2H), 1.04 (s, 6H); ¹³C NMR (100 MHz, CDCl₃) δ 191.4, 155.2, 140.4, 138.2, 134.0, 131.5, 131.3, 130.6, 129.5, 129.2, 128.1, 39.64, 34.45 33.28, 29.20, 22.09, 21.21, 19.38, 13.40.

NMR assignment was previously reported.[65]

Supplementary Material

Refer to Web version on PubMed Central for supplementary material.

Acknowledgements

References

[1]. Dupe V, Ghyselinck NB, Thomazy V, Nagy L, Davies PJ, Chambon P, Mark M, Dev Biol 1999, 208, 30–43. [PubMed: 10075839]

[2]. Canete A, Cano E, Munoz-Chapuli R, Carmona R, Nutrients 2017, 9.

[3]. Palczewski K, J Biol Chem 2012, 287, 1612–1619. [PubMed: 22074921]

[4]. von Lintig J, Kiser PD, Golczak M, Palczewski K, Trends Biochem Sci 2010, 35, 400–410. [PubMed: 20188572]

[5]. Hofmann L, Palczewski K, Prog Retin Eye Res 2015, 49, 46–66. [PubMed: 26187035]

[6]. Jiang L, Dong R, Ying M, He Q, Cao J, Yang B, Br J Pharmacol 2018, 175, 4285–4294. [PubMed: 30298911]

[7]. Khillan JS, Nutrients 2014, 6, 1209–1222. [PubMed: 24662164]

[8]. Rollman O, Vahlquist A, J Invest Dermatol 1986, 86, 384–389. [PubMed: 2943822]

[9]. Pinto NR, Applebaum MA, Volchenboum SL, Matthay KK, London WB, Ambros PF, Nakagawara A, Berthold F, Schleiermacher G, Park JR, Valteau-Couanet D, Pearson AD, Cohn SL, J Clin Oncol 2015, 33, 3008–3017. [PubMed: 26304901]

[10]. Handkiewicz-Junak D, Roskosz J, Hasse-Lazar K, Szpak-Ulczok S, Puch Z, Kukulska A, Olczyk T, Piela A, Paliczka-Cieslik E, Jarzab B, Thyroid Res 2009, 2, 8. [PubMed: 19646277]

[11]. Jones H, Blanc D, Cunliffe WJ, The Lancet 1980, 316, 1048–1049.

[12]. Uray IP, Dmitrovsky E, Brown PH, Semin Oncol 2016, 43, 49–64. [PubMed: 26970124]

[13]. Kiser PD, Golczak M, Maeda A, Palczewski K, Biochim Biophys Acta 2012, 1821, 137–151. [PubMed: 21447403]

[14]. Kiser PD, Palczewski K, Annu Rev Vis Sci 2016, 2, 197–234. [PubMed: 27917399]

[15]. Kahremany S, Kubas A, Tochtrop GP, Palczewski K, Dalton Trans 2019, 48, 10581–10595. [PubMed: 31218312]

[16]. Waldeck DH, Chemical Reviews 1991, 91, 415–436.

[17]. Arai T, Tokumaru K, Chemical Reviews 1993, 93, 23–39.

[18]. Denny M, Liu RSH, J. Am. Chem. Soc 1977, 99, 4865–4867. [PubMed: 874236]

[19]. Muramoto Y, Kimura M, Nouda S, Semiconductor Science and Technology 2014, 29, 084004.

[20]. Kalajian TA, Aldoukhi A, Veronikis AJ, Persons K, Holick MF, Sci Rep 2017, 7, 11489. [PubMed: 28904394]

[21]. Ganapathy S, Liu RSH, 1992, 56, 959–964.

[22]. Chen S, Yu Y-L, Wang J-H, Analytica Chimica Acta 2018, 999, 13–26. [PubMed: 29254563]

[23]. Dawson W, Abrahamson EW, J. Phys. Chem 1962, 66, 2542–2547.

[24]. Salem L, Science 1976, 191, 822. [PubMed: 1251196]

[25]. Singh K, Staig SJ, Weaver JD, J Am Chem Soc 2014, 136, 5275–5278. [PubMed: 24678625]

[26]. Singh A, Fennell CJ, Weaver JD, Chem Sci 2016, 7, 6796–6802. [PubMed: 28042465]

[27]. Walker AG, Radda GK, Nature 1967, 215, 1483.

[28]. Löwdin PO, The Journal of Chemical Physics 1950, 18, 365–375.

[29]. Polli D, Altoè P, Weingart O, Spillane KM, Manzoni C, Brida D, Tomasello G, Orlandi G, Kukura P, Mathies RA, Garavelli M, Cerullo G, Nature 2010, 467, 440. [PubMed: 20864998]

[30]. Johnson PJM, Farag MH, Halpin A, Morizumi T, Prokhorenko VI, Knoester J, Jansen TLC, Ernst OP, Miller RJD, J Phys Chem B 2017, 121, 4040–4047. [PubMed: 28358485]

[31]. Johnson PJM, Halpin A, Morizumi T, Prokhorenko VI, Ernst OP, Miller RJD, Nature Chemistry 2015, 7, 980.

[32]. Frutos LM, Andruniow T, Santoro F, Ferre N, Olivucci M, Proc Natl Acad Sci U S A 2007, 104, 7764–7769. [PubMed: 17470789]

[33]. Gozem S, Huntress M, Schapiro I, Lindh R, Granovsky AA, Angeli C, Olivucci M, J Chem Theory Comput 2012, 8, 4069–4080. [PubMed: 26605574]

[34]. Yamaguchi K, Chemical Physics Letters 1975, 33, 330–335.

[35]. Noodleman L, The Journal of Chemical Physics 1981, 74, 5737–5743.

[36]. Liu RSH, Asato AE, Denny M, Journal of the American Chemical Society 1983, 105, 4829–4830.

[37]. Oelgemöller M, Hoffmann N, Organic & Biomolecular Chemistry 2016, 14, 7392–7442. [PubMed: 27381273]

[38]. Politano F, Oksdath-Mansilla G, Organic Process Research & Development 2018, 22, 1045–1062.

[39]. Gao S, Kahremany S, Zhang J, Jastrzebska B, Querubin J, Petersen-Jones SM, Palczewski K, Molecular Pharmacology 2018, 93, 438. [PubMed: 29453250]

[40]. Van Hooser JP, Aleman TS, He Y-G, Cideciyan AV, Kuksa V, Pittler SJ, Stone EM, Jacobson SG, Palczewski K, Proceedings of the National Academy of Sciences 2000, 97, 8623.

[41]. Gearhart PM, Gearhart C, Thompson DA, Petersen-Jones SM, Archives of Ophthalmology 2010, 128, 1442–1448. [PubMed: 20837787]

[42]. Maeda A, Golczak M, Palczewski K, Maeda T, Cideciyan AV, Jacobson SG, Aleman TS, Human Molecular Genetics 2009, 18, 2277–2287. [PubMed: 19339306]

[43]. Hara T, Hara R, Nature 1967, 214, 573–575. [PubMed: 6036171]

[44]. Willcott MR, J. Am. Chem. Soc 2009, 131, 13180–13180.

[45]. Baker BY, Gulati S, Shi W, Wang B, Stewart PL, Palczewski K, Methods Enzymol 2015, 557, 439–458. [PubMed: 25950977]

[46]. Cogan U, Kopelman M, Mokady S, Shinitzky M, Eur J Biochem 1976, 65, 71–78. [PubMed: 945163]

[47]. Okada T, Matsuda T, Kandori H, Fukada Y, Yoshizawa T, Shichida Y, Biochemistry 1994, 33, 4940–4946. [PubMed: 8161555]

[48]. Neese F, Vol. 8, 2018, p. e1327.

[49]. Becke AD, The Journal of Chemical Physics 1993, 98, 5648–5652.

[50]. Lee C, Yang W, Parr RG, Physical Review B 1988, 37, 785–789.

[51]. Vosko SH, Wilk L, Nusair M, Canadian Journal of Physics 1980, 58, 1200–1211.

[52]. Grimme S, Ehrlich S, Goerigk L, J Comput Chem 2011, 32, 1456–1465. [PubMed: 21370243]

[53]. Grimme S, Antony J, Ehrlich S, Krieg H, J Chem Phys 2010, 132, 154104. [PubMed: 20423165]

[54]. Weigend F, Ahlrichs R, Phys Chem Chem Phys 2005, 7, 3297–3305. [PubMed: 16240044]

[55]. Eichkorn K, Weigend F, Treutler O, Ahlrichs R, Theoretical Chemistry Accounts 1997, 97, 119–124.

[56]. Eichkorn K, Treutler O, Öhm H, Häser M, Ahlrichs R, Chemical Physics Letters 1995, 242, 652–660.

[57]. Izsak R, Neese F, J Chem Phys 2011, 135, 144105. [PubMed: 22010696]

[58]. Maitra NT, The Journal of Chemical Physics 2016, 144, 220901. [PubMed: 27305987]

[59]. Casida ME, Huix-Rotllant M, Annual Review of Physical Chemistry 2012, 63, 287–323.

[60]. Bannwarth C, Grimme S, Computational and Theoretical Chemistry 2014, 1040–1041, 45–53.

[61]. de Souza B, Neese F, Izsák R, The Journal of Chemical Physics 2018, 148, 034104. [PubMed: 29352790]

[62]. Harvey JN, Aschi M, Schwarz H, Koch W, Theoretical Chemistry Accounts 1998, 99, 95–99.

[63]. Albert K, Schlotterbeck G, Braumann U, Händel H, Spraul M, Krack G, Angew. Chem. Int. Ed. Engl 1995, 34, 1014–1016.

[64]. Choi YH, Kim HK, Wilson EG, Erkelens C, Trijzelaar B, Verpoorte R, Anal. Chim. Acta 2004, 512, 141–147.

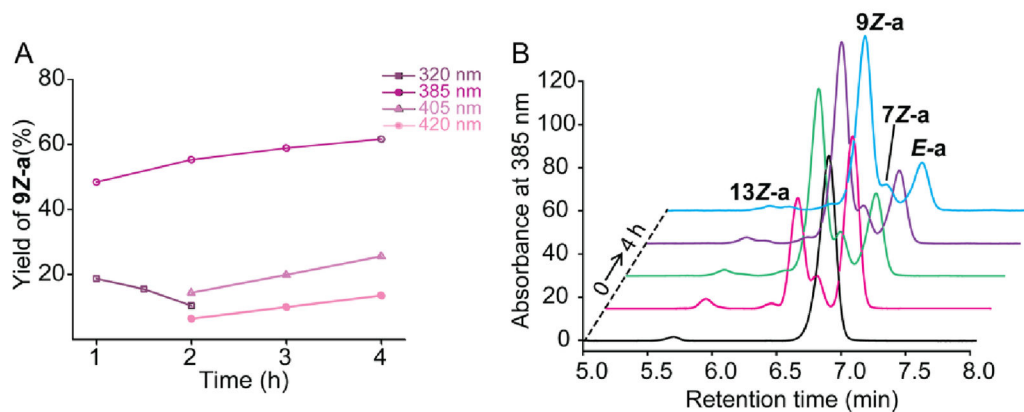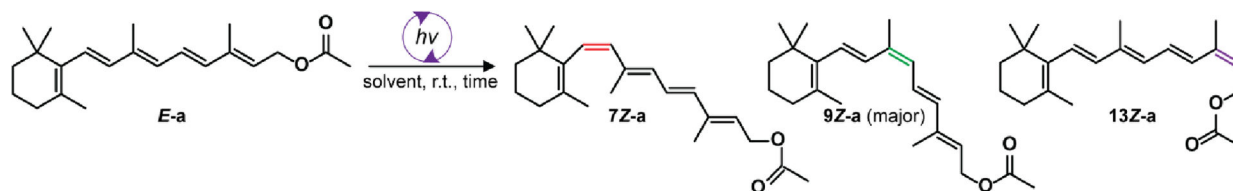[65]. Wang KW, Wang SW, Du QZ, Magn. Reson. Chem 2013, 51, 435–438. [PubMed: 23630063]

Figure 1.
Screening of wavelength bands for the isomerization of *E* to *Z* retinyl acetate. A) The yield of **9Z-a** using different wavelengths over 4 h. B) HPLC chromatograms of all-*trans* to 9-*cis* isomer after 0 (black), 20 min (pink), 1 (green), 2 (purple), and 4 (blue) h irradiation at 385 nm. Peak **13Z-a** represents 13-*cis*, Peak **9Z-a** represents 9-*cis*, Peak **7Z-a** represents 7-*cis*, and Peak **E-a** represents all-*trans*.
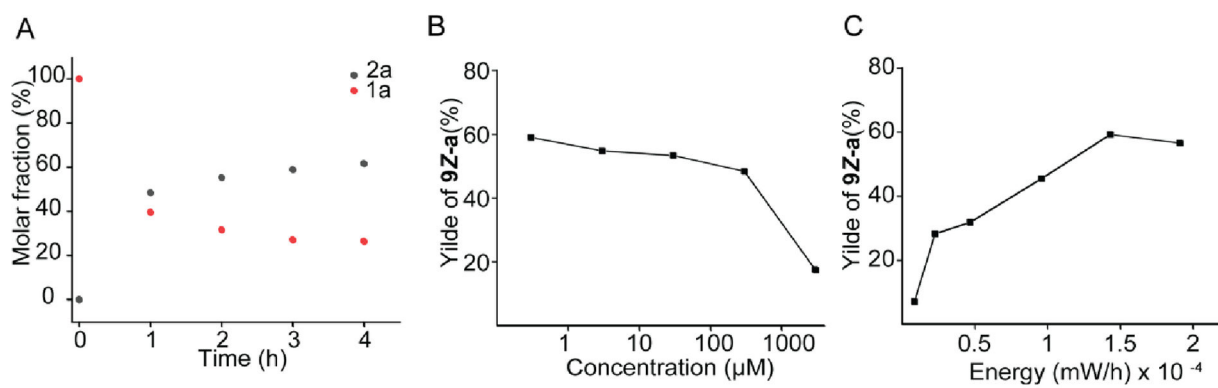
Figure 2.
A) Reaction progress monitoring the isomerization of all-*trans*-retinyl acetate to the 9-*cis* isomer. B) Dose dependency of *E* retinyl acetate. C) Energy level measurements.
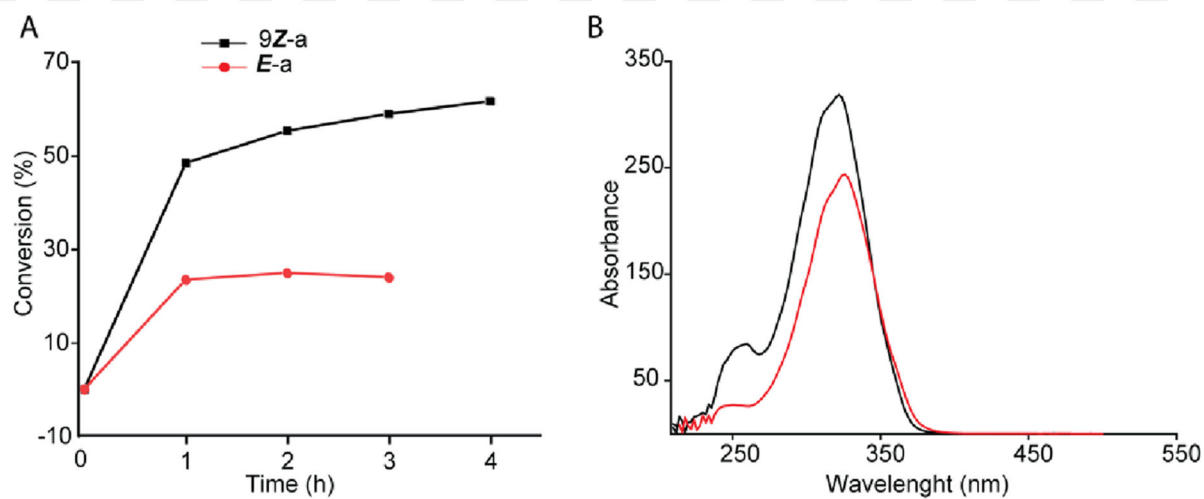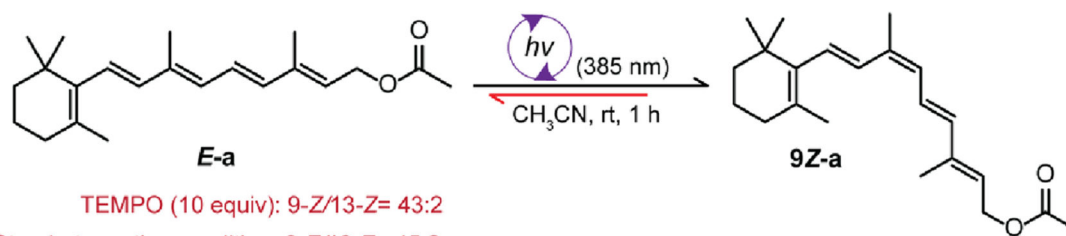
Figure 3.
Relationship between the distribution of *cis*-retinyl acetate isomers. A) Time course of the reaction from *E* to *Z* and backward. B) Absorbance spectra of all-*trans* **E-a** and 9-*cis* **9Z-a** isomers.
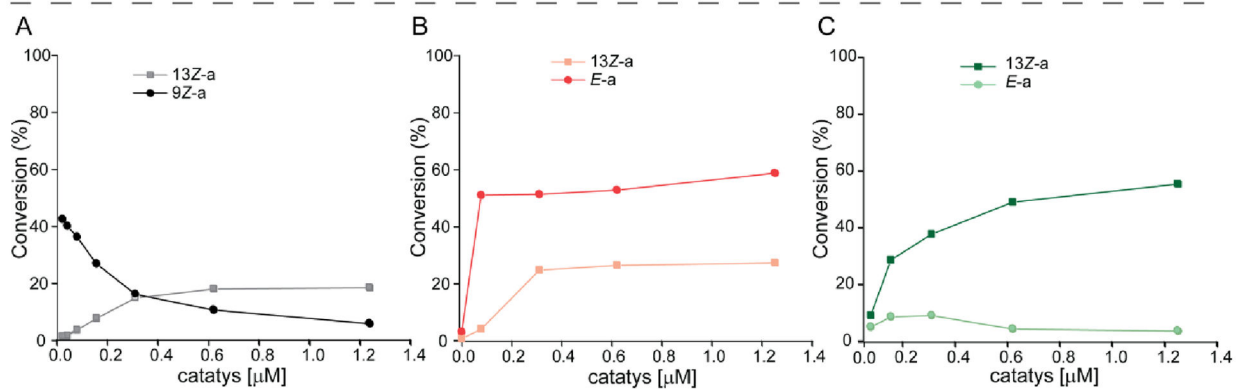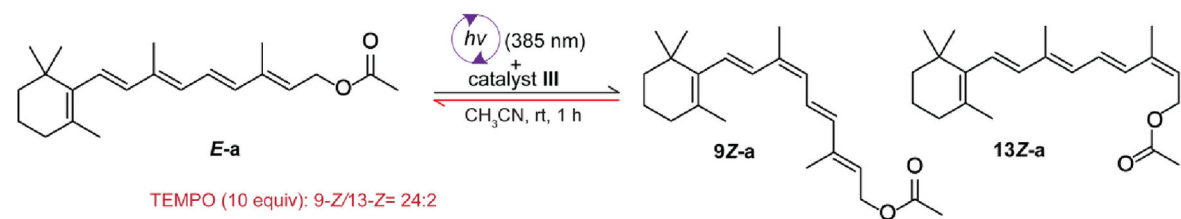
Figure 4.
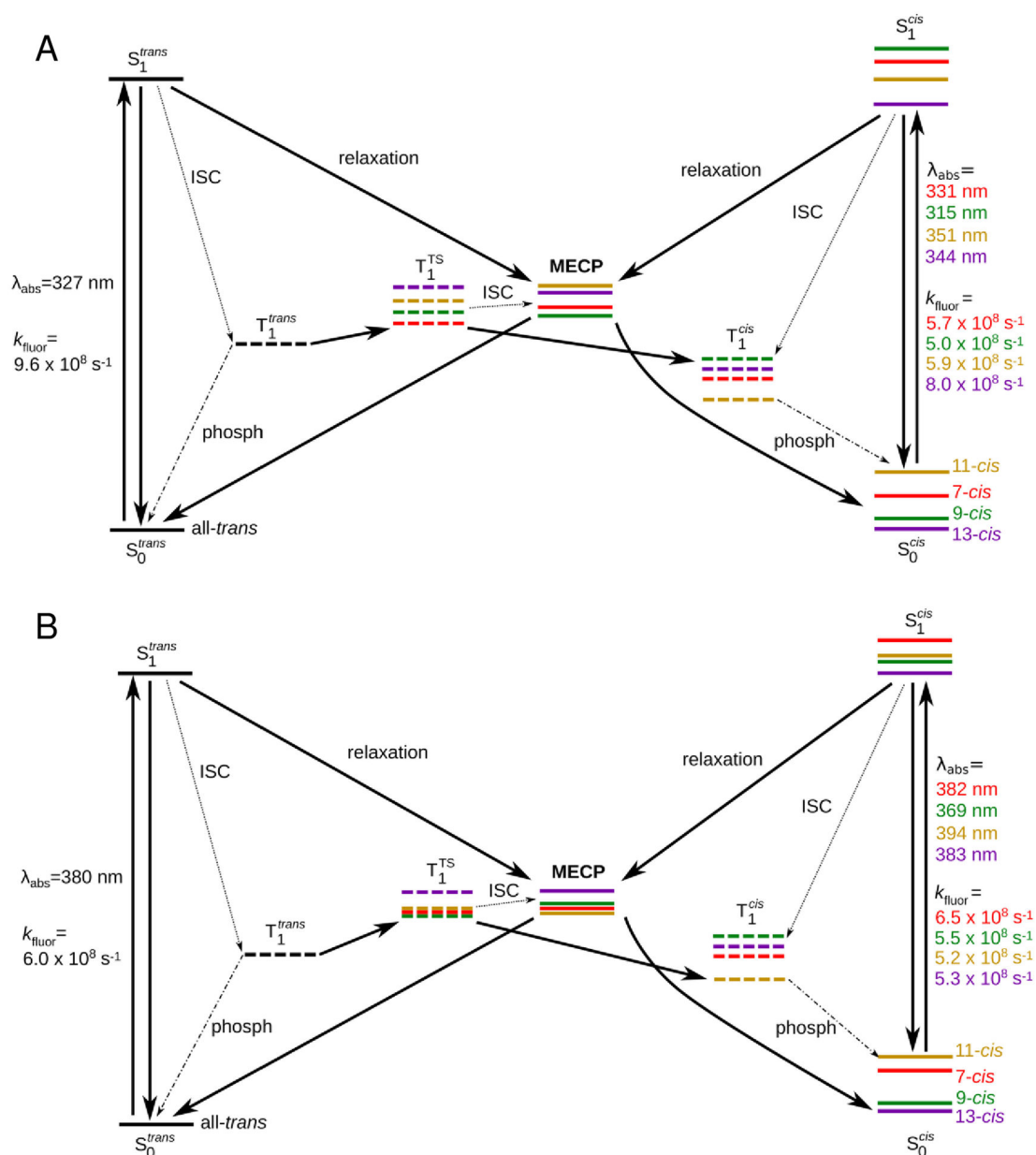Exploring a catalyst effect on the distribution of *cis*-retinyl acetate isomers.

Figure 5.
Computed Jablonski diagrams of the photochemical isomerizations of (A) retinyl acetate *E-a* and (B) retinal *E-d*. Singlet and triplet states are represented with solid and dashed lines. Color code denotes the isomer of interest: all-*trans* (black), 7-*cis* (red), 9-*cis* (green), 11-*cis* (yellow), 13-*cis* (violet). Fast processes are represented with solid arrows (absorption, emission, relaxation), while slow processes are depicted with dotted lines (intersystem crossing, ISC) or dot-dash lines (phosphorescence, phosph). T_1^{TS} denotes transition states for rotations around C=C bonds in the first triplet state and MECP is the minimum energy crossing point that approximates the true conical intersection point between S_0 and S_1 surfaces. Computed absorption wavelength (λ_{max}) maxima and the fluorescence rates (k_{fluor}) are provided for all ground state isomers.
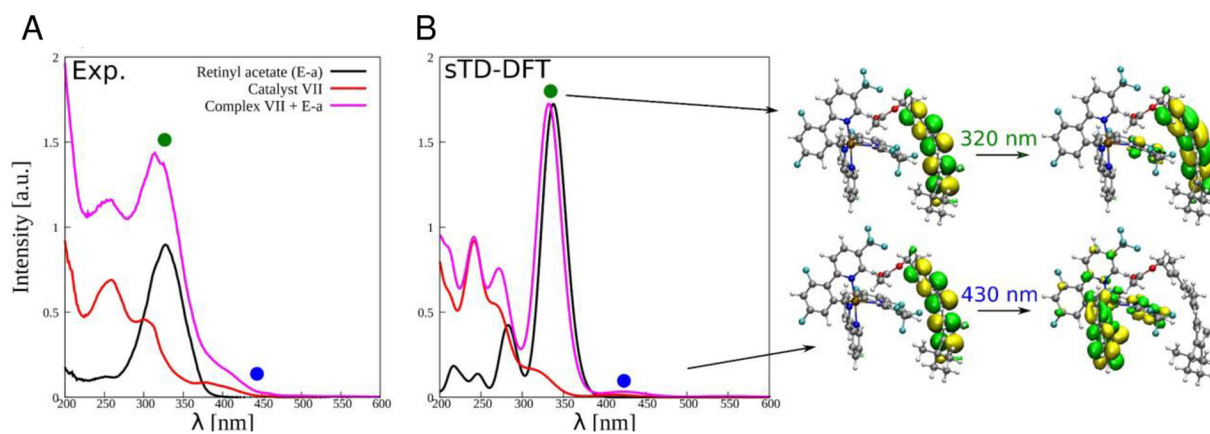
Figure 6.
Experimental and calculated UV-VIS spectra for retinyl acetate *E*-a and in a complex with catalyst **III.** A) Experimental spectra of the retinyl acetate *E*-a (black), catalyst **III** (red) and the complex of the two (magenta). B) Computed spectra of the retinyl acetate *E*-a. On the right: one-electron orbital picture of two key transitions.
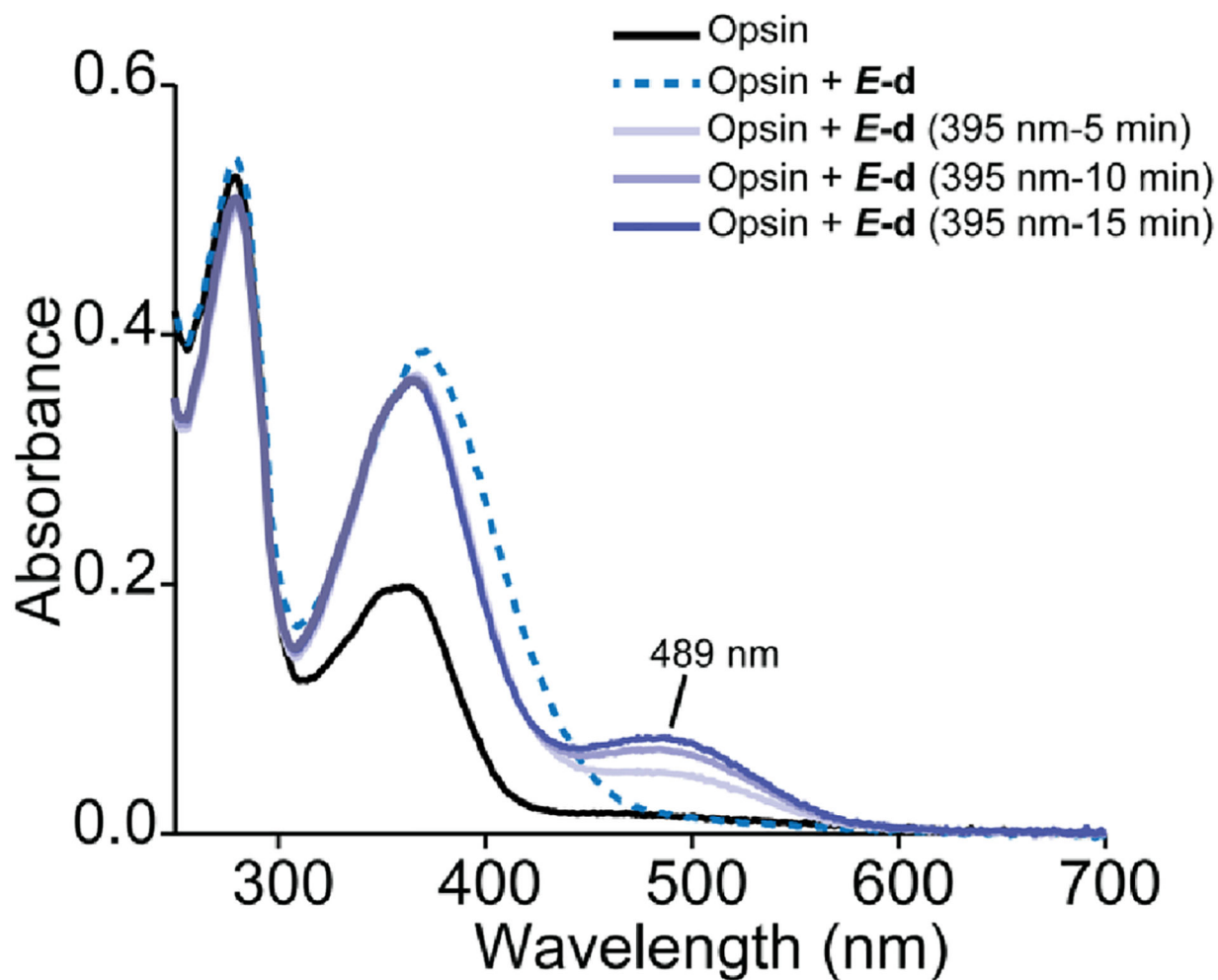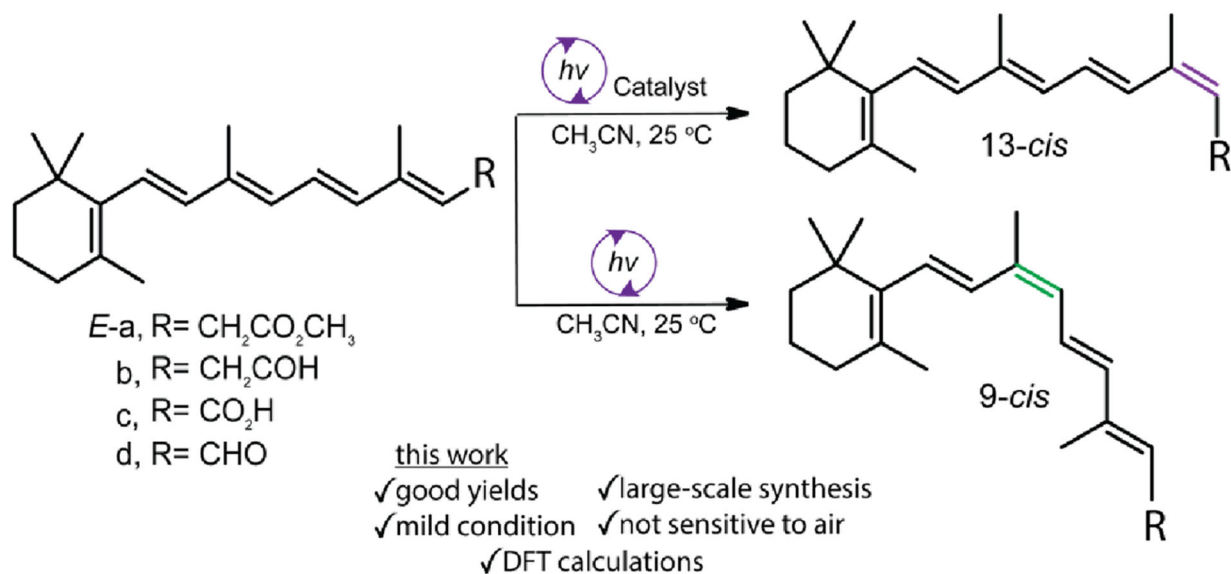
Figure 7.
UV-Vis absorption spectra of opsin (black) and opsin with addition of all-*trans*-retinal **E-a**
(blue dashed) after irradiation with 395 nm UV light for 5 min, 10 min and 15 min.

Scheme 1.
Photoisomerization of retinoids in two different pathways. Top arrow: isomerization with monochromatic UV light in the presence of catalyst produces mainly 13-*cis* among the *cis* isomers. Bottom arrow: isomerization with monochromatic UV light produces mainly the 9-*cis* among the *cis* isomers.
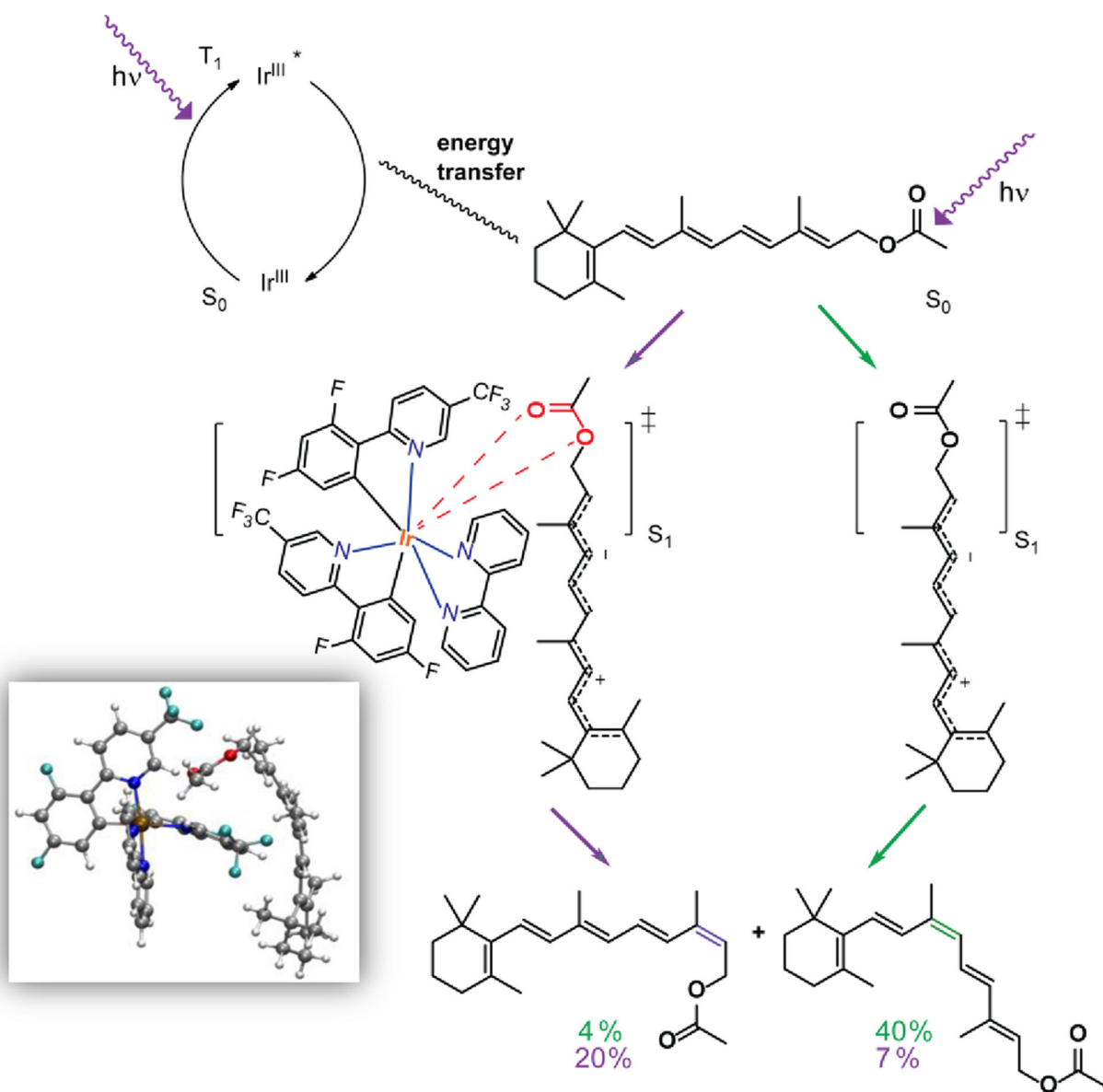
Scheme 2.
Theoretical reaction pathway for the *Z*-isomerization of all-*trans*-retinyl acetate **E-a**.
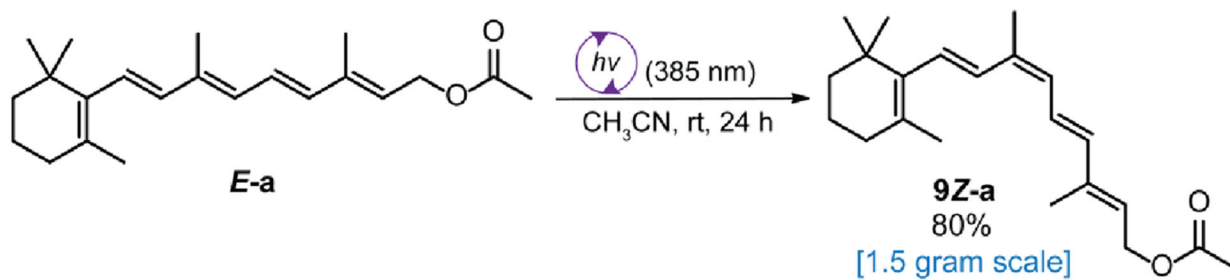
Scheme 3.
Gram-scale synthesis of 9-cis-retinyl acetate **9Z-a**.

Table 1.

Study of the reaction conditions.

					Product distribution ratio		
Entry	Solvent	Atmosphere	Wavelength (nm)	Conversion (%)	7Z-a	9Z-a	13Z-a
1	C_6H_{14}	Air	385	13 ± 0.5	-	1	0.4
2	CH_3CN	Air	385	66 ± 3	0.2	1	0.05
3	C_2H_5OH	Air	385	69 ± 4	0.1	1	0.07
4	EtOAC	Air	385	57 ± 3	0.5	1	0.1
5	CH_3CN/H_2O (20/1)	Air	385	64 ± 2	0.3	1	-
6	CH_3CN/H_2O (1/20)	Air	385	27 ± 1	-	1	0.1
7	CH_3CN	N_2	385	64 ± 2	0.2	1	0.03
8	CH_3CN	Air	320	34 ± 5	0.1	1	0.6
9	CH_3CN	Air	405	18 ± 5	0.2	1	0.1
10	CH_3CN	Air	420	8 ± 2	0.2	1	0.5
11	CHCN/DMSO (20/1)	Air	385	65 ± 2.5	0.2	1	0.02
12	CH_3CN	Air	(in the dark)	0	-	-	-

Reactions were carried out with all-*trans*-retinyl acetate (0.1 mmol) at room temperature for 1 h. Each percent conversion is averaged from n 2 reactions and was determined by HPLC analysis. Uncertainties are reported as half the range of replicate results.

Table 2.

Z-isomerization of all-*trans*-retinoid using different UV wavelengths.

				Product distribution ratio			
Entry	**Substrate**	**Wavelength (nm)**	**Conversion (%)**	**7Z**	**9Z**	**11Z**	**13Z**
1	**E-b**	420	73 ± 2	-	1	1.2	0.6
2	**E-c**	385	46 ± 4	-	1	-	-
3	**E-d**	395	58 ± 1	0.1	1	1.7	1.3

Reactions were carried out with all-*trans*-retinoid (0.1 mmol) for 1 h at room temperature. Each percent conversion was averaged from n ≥ 2 reactions and was determined by HPLC analysis. Uncertainties are reported as half the range of replicate results.
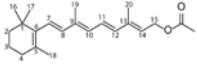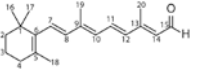
Table 3.

Z-isomerization of all-*trans*-retinoid using UV irradiation and catalyst **III**.

Entry	Substrate	Wavelength (nm)	Conversion (%)	Product distribution ratio			
				7Z	**9Z**	**11Z**	**13Z**
1	**E-a**	385	35 ± 2.5	0.2	1	-	0.04
2	**E-b**	420	60 ± 3	-	1	1.4	1.1
3	**E-c**	385	0	-	-	-	-
4	**E-d**	395	52 ± 3	0.2	1	1.6	1.4

Reactions were carried out with all-*trans*-retinoid (0.1 mmol) and catalyst (5 mol %) for 1 h at room temperature and products quantified by HPLC. Each percent conversion was averaged from n ≥ 2 reactions. Uncertainties are reported as half the range of replicate results. On the right: structure of the tested catalysts.

Table 4.

Selected geometric and electronic structure parameters for two representative molecules studied: retinyl acetate (*E*-a) and retinal (*E*-d). Carbon atom numbering is given for both structures.

	E-a	*E*-d
Selected C-C bond lengths [Å]		
C^7-C^8	1.343	1.345
C^8-C^9	1.453	1.449
C^9-C^{10}	1.359	1.361
C^{10}-C^{11}	1.436	1.430
C^{11}-C^{12}	1.351	1.354
C^{12}-C^{13}	1.454	1.445
C^{13}-C^{14}	1.348	1.359
HOMO / LUMO Loewdin orbital atomic populations [%]		
C^7	12.6 / 11.0	11.6 / 7.9
C^8	6.9 / 6.1	8.1 / 3.6
C^9	11.6 / 11.7	8.4 / 9.1
C^{10}	12.4 / 9.4	11.7 / 5.1
C^{11}	8.2 / 11.5	5.3 / 11.0
C^{12}	12.6 / 13.7	11.0 / 8.6
C^{13}	4.0 / 7.2	2.6 / 10.1
C^{14}	10.4 / 12.8	8.0 / 9.8
Relative local polarization change upon HOMO → LUMO excitation ($LPC_{HOMO \rightarrow LUMO}$) [%]		
C^7-C^8	14.0	22.9
C^9-C^{10}	187.5	21.2
C^{11}-C^{12}	50	57.9
C^{13}-C^{14}	12.5	94.4